Disturbance-free phase-shifting laser diode interferometer using adaptive feedback control

Takamasa Suzuki,* Tsutomu Takahashi, and Osami Sasaki

Niigata University, Faculty of Engineering, 8050 Ikarashi 2, Niigata 950-2181, Japan

*Corresponding author: takamasa@eng.niigata-u.ac.jp

Received 29 June 2009; revised 29 August 2009; accepted 20 September 2009; posted 21 September 2009 (Doc. ID 113548); published 5 October 2009

A feedback-control-equipped phase-shifting laser diode interferometer that eliminates external disturbance is proposed. The feedback loop is stabilized by adaptive control of the polarity of the interference signal. Conventional phase-shifting interferometry can be used with the feedback control, resulting in simplified signal processing and accurate measurement. Several experiments confirm the stability of the feedback control with a measurement repeatability of 1.8 nm. © 2009 Optical Society of America

OCIS codes: 120.3180, 120.3940, 120.5050, 120.6660, 140.2020.

1. Introduction

Wavelength-tunability is one of the useful properties of a laser diode (LD) [1], since it allows phase control in an interference signal [2]. As the popularity of LD-based interferometric measuring devices grows, so does the need for precision, robustness, and simplicity in signal processing. We can classify the wavelength-tunability-based modulating techniques of the LD into phase-shifting interferometry (PSI) [3], heterodyne interferometry [4], and sinusoidal phase-modulating interferometry (SPMI) [5,6] on the basis of the modulating waveform (Fig. 1). While all three approaches provide accurate phase measurement, they are susceptible to external disturbances. A feedback (FB) control technique has been applied to SPMI to reduce the effects of external disturbances [7]. Since the dc component of the interference signal is not affected by the modulating process in SPMI or heterodyne interferometry, it is not difficult to install the FB system in the interferometer. It is particularly easy to generate the FB signal in SPMI because the modulation signal is continuous. In our previously proposed system, which was developed using SPMI [8], the phase-locked technique was used to shift the phase. Exact phase information was required as the FB signal. The phase-locked technique gradually changes the phase in the interference signal, so that FB control can be easily applied. However, a long processing time is required in order to measure the surface profile while the effect of external disturbances is being reduced.

However, if the FB technique is installed in conventional PSI, the processing time for phase shifting is reduced. In addition, the external disturbance is eliminated more efficiently because the response time of the FB loop is improved. A closed-loop phase-control system using an optical fiber has been proposed [9]. Although an argon-ion laser was used as a light source, stable and accurate phase control is achieved because the system is configured by taking a loop polarity into consideration. Yoshino and Yamaguchi [10] proposed closed-loop PSI with an LD. In their system, measurements are conducted by PSI, whereas the FB signal is detected by using the two-frequency optical heterodyne method; therefore, a complicated optical setup is required. On the other hand, if the FB signal can be generated from the interference signal during phase shifting, the optical setup can be simplified. However, the problem in this method is the polarity of the FB loop: the sign of the

0003-6935/09/295561-06$15.00/0

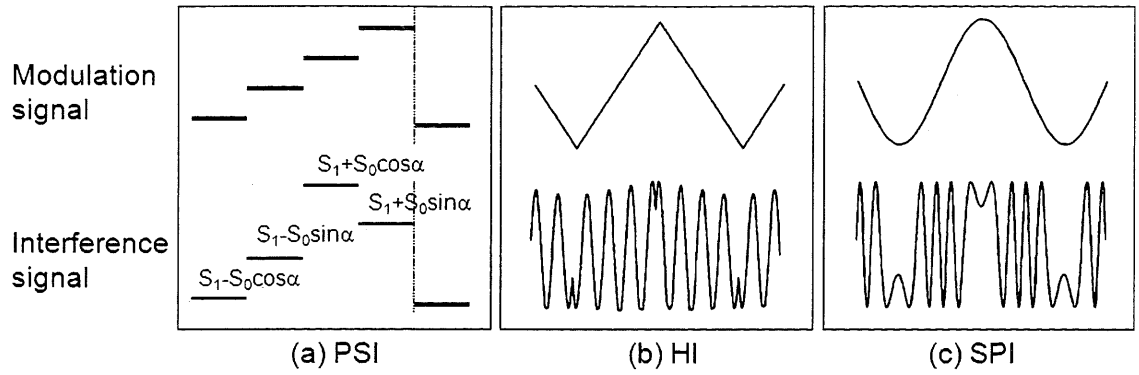

Fig. 1. Classifications of the modulating techniques with their modulating waveforms. HI, heterodyne interferometry.

FB control changes without notice from negative to positive during the modulating process, as will be discussed below. Therefore, it is difficult to implement FB control in PSI.

While signal processing in PSI is simple, as shown in Fig. 1(a), and it allows the measurement of a large area within a short period of time, it is necessary to consider the sequence in which captured fringe images are calculated. In this paper, we propose an FB-type PSI that uses adaptive FB control to maintain FB loop stability. Since the process of image capture using a CCD camera is synchronized with the phase shift, the order in which images are presented is definitely accurate, enabling disturbance-free signal processing to be carried out. We developed a prototype using a conventional Twyman–Green interferometer and measured the profiles of a solid surface. An experiment conducted by using this prototype confirmed the stability of the FB control with a measurement repeatability of 1.8 nm.

2. Principle

A. Phase Control in Interference Signal

The device setup is shown in Fig. 2. A conventional Twyman–Green LD interferometer is used as the optical system. The CCD camera captures a two-dimensional interference fringe containing the surface profile information of the object. The photodiode (PD) detects the temporal intensity change in the interference signal to generate the FB signal. When the phase of the interference signal on the PD is shifted by the FB control, the fringe on the CCD camera varies for the same amount of phase shift. Phase control of the interference signal detected by the PD is discussed to simplify the explanations that follow.

In an unbalanced LD interferometer, there is an interference signal

$$S = a + b\cos\alpha_0 \tag{1}$$

on the PD, where

$$\alpha_0 = 2\pi L/\lambda_0 \tag{2}$$

is the initial phase corresponding to the optical path difference L and wavelength λ_0. The coefficients a and b represent the background intensity and amplitude of the interference signal, respectively. In our proposed system, the FB controller simultaneously changes the wavelength λ_0 by λ_s and λ_c, using the wavelength tunability of the LD to, respectively, shift the phase and compensate for the change in optical path difference, d, that is induced by the external disturbance. If d is eliminated from the interference signal, the disturbance in the interference signal captured by the CCD camera is also eliminated.

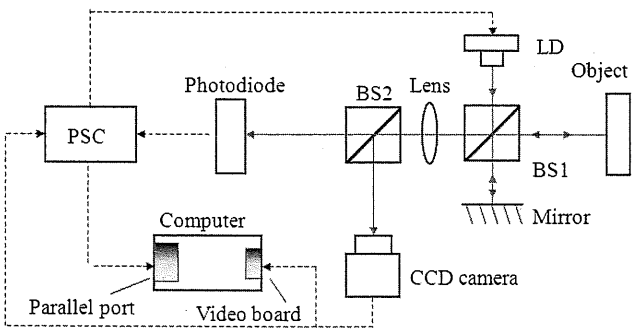

Fig. 2. (Color online) Schematic of the experimental setup. LD, laser diode; BS1, BS2, beam splitters; PSC, phase-shifting controller.

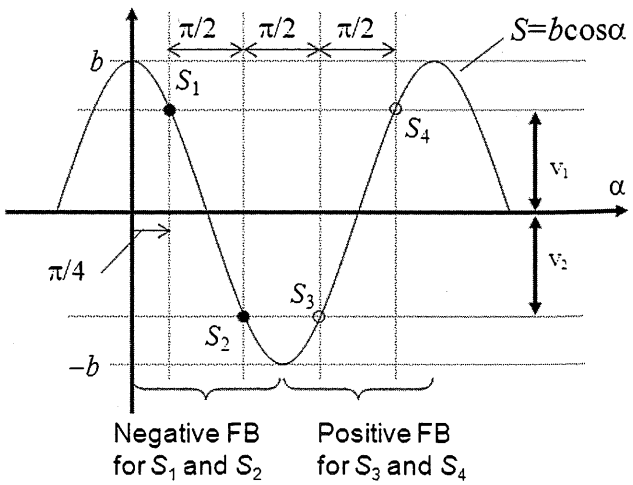

Fig. 3. Polarity of the FB control depending on the location of the operating point.

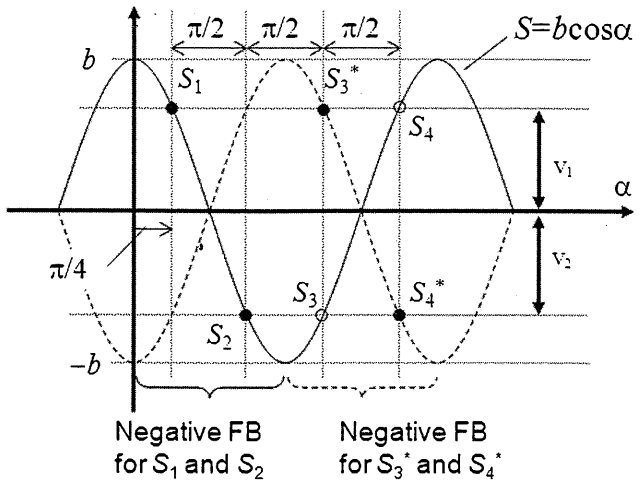

Fig. 4. Polarity of the FB control under adaptive control. Operating points S_1 and S_2 are on the original interference signal (solid curve), whereas $S_3{}^*$ and $S_4{}^*$ are on the inverted interference signal (dashed curve).

According to the above wavelength change, the phase is given by

$$\alpha_c = \frac{2\pi(L+d)}{\lambda_0 - \lambda_s + \lambda_c} = \frac{2\pi L}{\lambda_0} + \frac{2\pi L}{{\lambda_0}^2}\lambda_s + \frac{2\pi d}{\lambda_0} - \frac{2\pi L}{{\lambda_0}^2}\lambda_c. \quad (3)$$

In this calculation, the terms that contain small coefficients $d\lambda_s$ and $d\lambda_c$ were omitted. Because the last term $2\pi L\lambda_c/{\lambda_0}^2$ generated by the FB control cancels out the third term $2\pi d/\lambda_0$, external disturbance is automatically eliminated. At the same time, λ_s shifts the phase of the interference signal to the desired value.

B. Stabilization of Feedback Control

Figure 3 shows the polarity of the FB control depending on the location of the operating point. Because the reference of the control system is given by the intensity instead of the phase of the interference signal, in the present experiments the reference is set to $\sqrt{2}b/2$ ($\sim 0.707b$) or $-\sqrt{2}b/2$ ($\sim -0.707b$). Then, the operating points S_1–S_4 are represented by

$$S_i = b\cos\left[\frac{\pi}{4} + (i-1)\frac{\pi}{2}\right] \qquad (i = 1, 2, 3, 4), \quad (4)$$

where the dc term a is eliminated and the initial phase is maintained at $\pi/4$.

If negative FB is activated at the negative slope of the interference signal, the FB loop is stable at the operating points S_1 and S_2 shown in Fig. 3. On the other hand, the FB loop becomes unstable at S_3 and S_4 because positive FB is activated at the positive slope. However, as indicated in Fig. 4 by the dashed curve, if the interference signal is inverted when the operating point is located at S_3 or S_4, the operating point moves to $S_3{}^*$ and $S_4{}^*$, respectively. This operation is called adaptive control, and it allows the realization of negative FB at every operating point and maintains the stability of the FB loop.

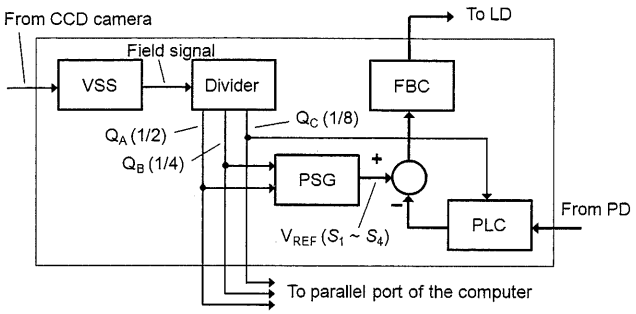

Fig. 5. Block diagram of the PSC. VSS, video synchronizing-signal separator; PSG, phase-shifting signal generator; PLC, polarity controller; FBC, FB controller.

3. Experiments

The experimental setup is shown in Fig. 2. The central wavelength and output power of the LD are

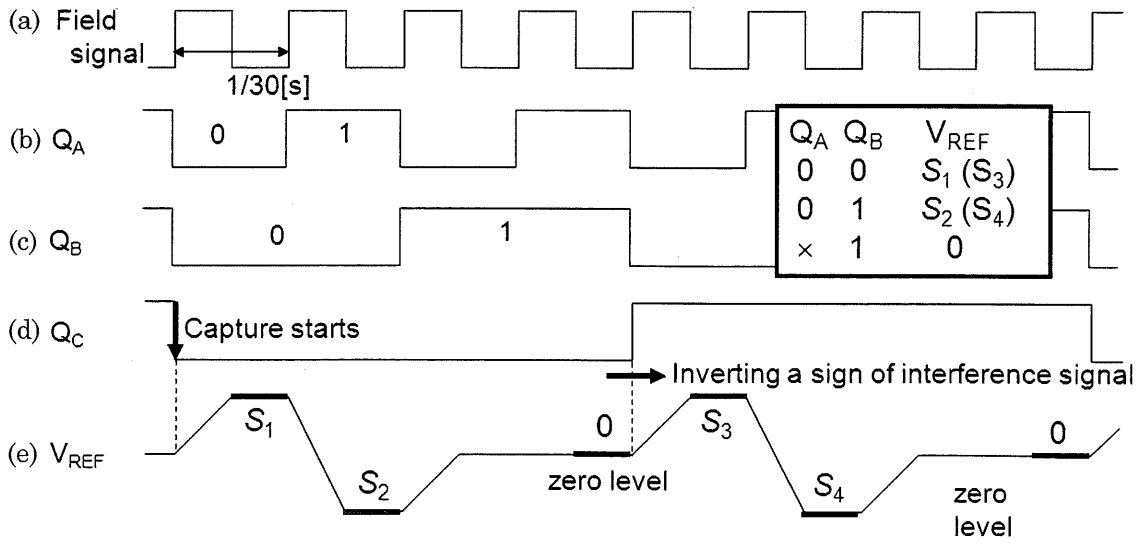

Fig. 6. Timing chart of adaptive FB control in the phase-shifting process.

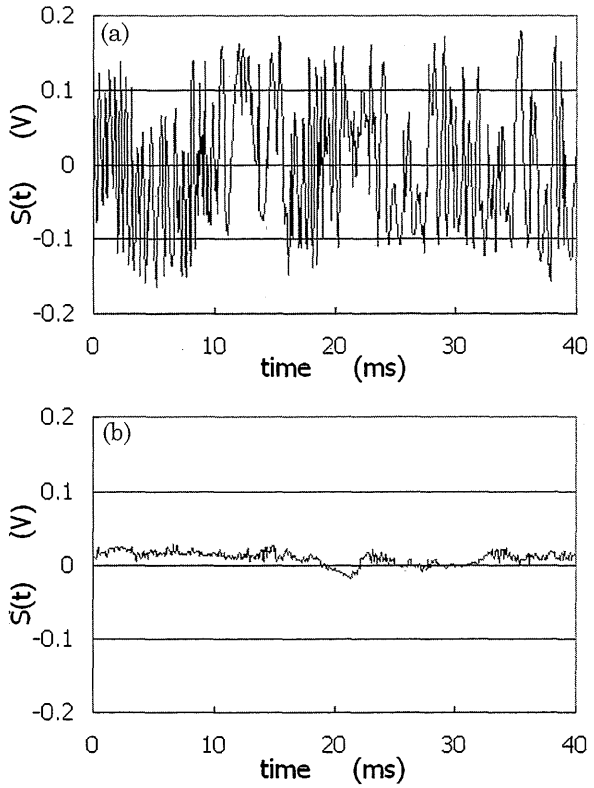

Fig. 7. (Color online) Temporal change in the interference signal observed at two states: (a) FB off and (b) FB on.

685 nm and 30 mW, respectively. The interferogram is divided by beam splitter BS2. A part of the interferogram is detected by the PD, which is covered by

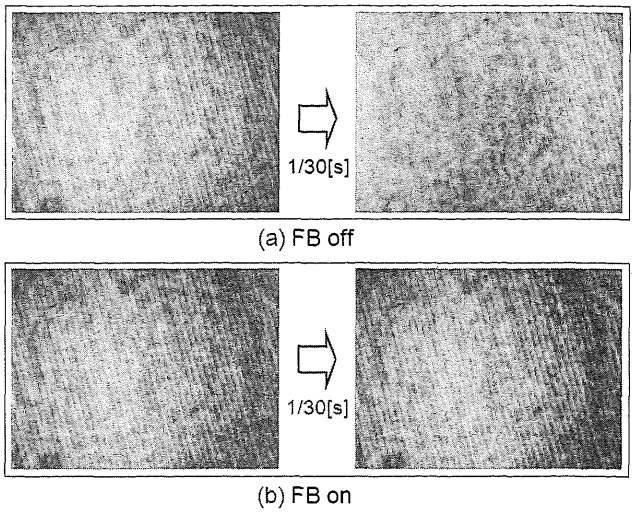

Fig. 8. Temporal change in the interferogram observed at two states: (a) FB off and (b) FB on.

the pinhole (whose diameter of ~0.5 mm is much smaller than the width of the fringe), to generate the FB signal. The fringe image is captured by using a standard CCD camera whose pixel size and exposure time are 6.35 μm (H) × 7.40 μm (V) and 10 μs, respectively. The lens after BS1 triple magnifies the image. The video signal from the CCD camera is fed to both the video board and the phase-shifting controller (PSC) so that the phase shift can be synchronized with the process of image capture.

Figure 5 shows the block diagram of the PSC. The video synchronizing-signal separator (VSS) extracts

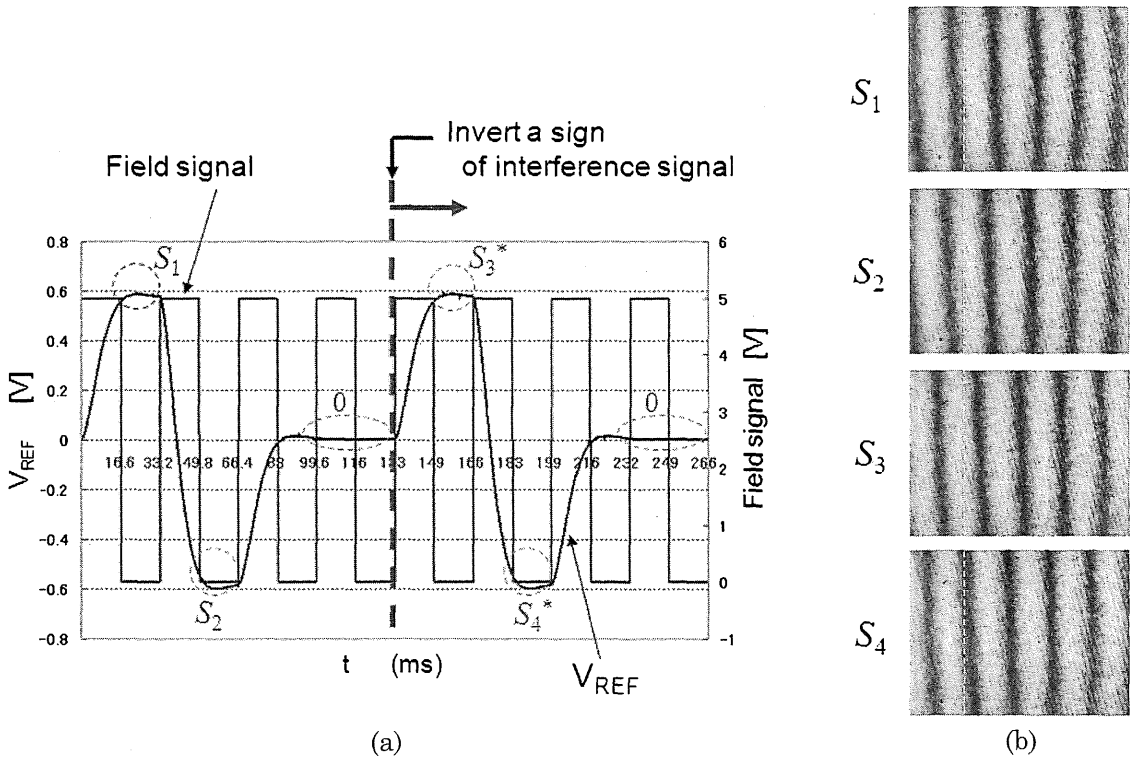

Fig. 9. (Color online) Observation of (a) phase-shifting process in the PSC and (b) phase-shifted interferograms.

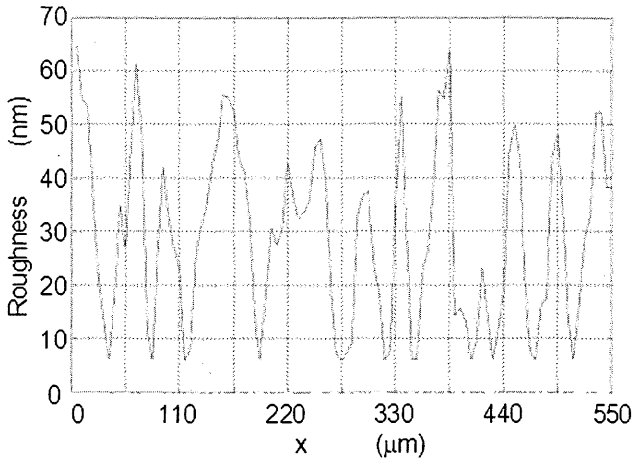

Fig. 10. (Color online) Two-dimensional trace of a diamond-turned aluminum disk measured by using the proposed system.

the field signal from the video signal. It is divided by 2 (Q_A), 4 (Q_B), and 8 (Q_C) by a divider. Q_A and Q_B are fed into the phase-shifting signal generator (PSG), which generates the reference signals (V_{REF}) for the FB control. These are defined in Eq. (4). One of the levels of V_{REF} is selected in accordance with the combination of Q_A and Q_B. The interference signal detected by the PD is fed to the polarity controller (PLC). If Q_C is low, the interference signal passes through the polarity controller without polarity change. If Q_C is high, the polarity of the interference signal is inverted to conduct adaptive FB control. The FB controller (FBC) regulates the interference signal according to the V_{REF} level. Although this FB control of the phase is implemented on the temporal interference signal detected by the PD, the phase shift is realized in the entire interferogram.

Figure 6 shows the timing chart of the signal processing in the above-mentioned PSC. The field signal shown in Fig. 6(a), which is separated from the video signal, is the base clock used for the phase shift. Q_A and Q_B shown in Fig. 6(b) and 6(c), respectively, and determines the level of the V_{REF} signal depending on the inset table. Q_C, shown in Fig. 6(d), is used for the image-capture trigger and the adaptive control. The sequence of captured images can be determined by detecting the trigger. The first two images are captured under negative FB control when the intensity of the interference signal is controlled at S_1 and S_2, respectively. The reference signal is set to zero once before the sign of the interference signal is inverted to maintain the stability of the FB loop. When Q_C becomes high, the sign of the interference signal is inverted and the next two images are captured at S_3 and S_4 under negative FB control.

First, the effect of disturbance elimination was confirmed in the FB control. The interference signal detected by the PD is traced in Fig. 7. When the FB control was not activated, the interference signal fluctuated significantly, as shown in Fig. 7(a). After activating the FB control, however, the interference signal stabilized, as shown in Fig. 7(b), in which the phase variation fell within around ±0.1 rad in the observed time range of 40 ms. The interferogram captured using the CCD camera is shown in Fig. 8. When the FB control was switched off, the interferogram varied significantly in the time interval of 1/30 s, as shown in Fig. 8(a). However, when the FB control was switched on, the image was very stable and no distinct differences were observed between the two images (Fig. 8(b)) because the phase was controlled within ±0.1 rad in the time interval of 1/30 s, as indicated in Fig. 7(b). These observations confirm that the FB control installed in our system worked as well as expected.

Next, the phase-shifting process was verified by observing V_{REF} and the phase-shifted fringes. The observed V_{REF} is traced with the field signal in Fig. 9(a). The time period of the rectangular field signal is 1/30 s, which conforms to National Television System Committee (NTSC) standards. The evolution of V_{REF} exhibits the same change as that shown in Fig. 6(e). The transit speed of V_{REF} is taken into account so that the stability of the FB loop is preserved. The phase-shifted interferograms are shown in Fig. 9(b). Each image is captured when the level of V_{REF} is S_1, S_2, $S_3{}^*$, and $S_4{}^*$. This indicates that a

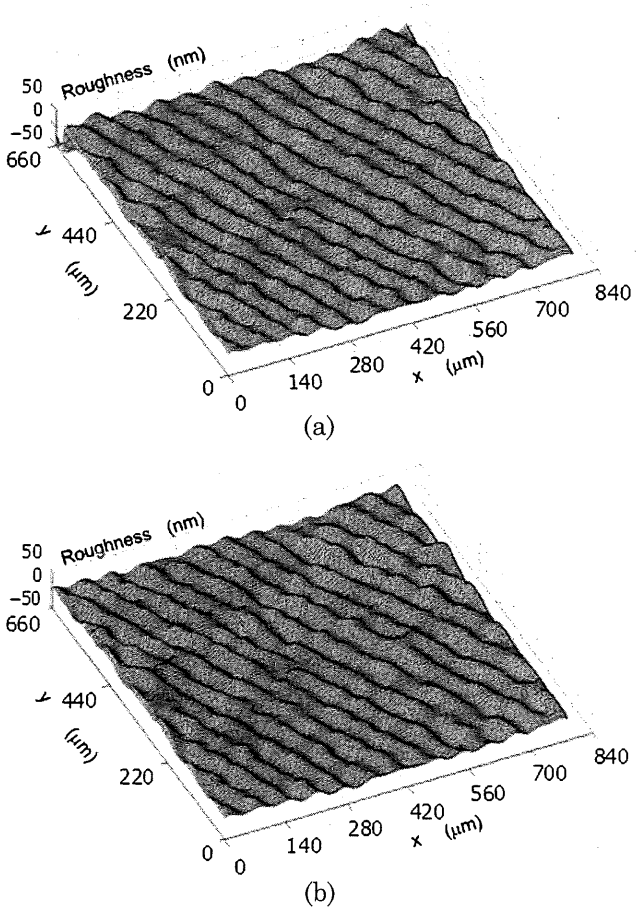

Fig. 11. Three-dimensional surface profile of an object measured by using the proposed system. The time interval of the measurements between (a) and (b) is 10 min.

phase shift of exactly $\pi/2$ is realized with this adaptive FB control.

Under adaptive FB control, surface-profile measurement was conducted on a diamond-turned aluminum disk with a cutting pitch of $40\,\mu$m. All measurements were carried out on an iron plate placed on a wooden desk. The FB loop was stabilized with the adaptive control, resulting in a highly accurate interferometric measurement that was insensitive to external disturbances. The two-dimensional trace measured by the proposed system is shown in Fig. 10. The pitch and roughness of $\sim$35 nm agreed well with the result verified by a Talystep profilometer [11]. The three-dimensional profile shown in Fig. 11 exhibits a periodic structure determined by the cutting pitch. The image order is exactly discriminated with the synchronous signal Q_C. We processed the images by weak low-pass filtering. While the time interval of the measurements between Figs. 11(a) and 11(b) was 10 min, these images correspond to each other. Additional measurements confirmed that the repeatability of the measurements in our proposed system was 1.8 nm.

4. Conclusions

In the present study, a phase-shifting interferometer equipped with a feedback (FB) controller was proposed and demonstrated. After applying the principles of disturbance elimination and adaptive control, the signal processing procedure was experimentally validated. It was observed that instability of the FB control in the phase-shifting process could be avoided by implementing adaptive control. In our prototype, a measurement repeatability of $\sim$1.8 nm was confirmed through the measurements of the solid surface profile. The system proposed in this paper is easily applicable to other major two-beam interferometers such as those of the Mach–Zehnder type and the Fizeau type. In addition, it is capable of measuring transparent objects such as lenses and thin films.

References

1. K. Tatsuno and Y. Tsunoda, "Diode laser direct modulation heterodyne interferometer," Appl. Opt. **26**, 37–40 (1987).
2. K. Hotate and D.-T. Jong, "Quasiheterodyne optical fiber sensor with automated adjustment of the driving wave parameter," Appl. Opt. **26**, 2956–2961 (1987).
3. R. Onodera and Y. Ishii, "Frame rate phase-shifting interferometer with a frequency-modulated laser diode," Opt. Eng. **38**, 2045–2049 (1999).
4. J. Chen, Y. Ishii, and K. Murata, "Heterodyne interferometry with a frequency-modulated laser diode," Appl. Opt. **27**, 124–128 (1988).
5. O. Sasaki, T. Yoshida, and T. Suzuki, "Double sinusoidal phase-modulating laser diode interferometer for distance measurement," Appl. Opt. **30**, 3617–3621 (1991).
6. T. Suzuki, O. Sasaki, J. Kaneda, and T. Maruyama, "Real-time two-dimensional surface profile measurement in sinusoidal phase modulating laser diode interferometer," Opt. Eng. **33**, 2754–2759 (1994).
7. O. Sasaki, K. Takahashi, and T. Suzuki, "Sinusoidal phase modulating laser diode interferometer with a feedback control system to eliminate external disturbance," Opt. Eng. **29**, 1511–1515 (1990).
8. T. Suzuki, X. Zhao, and O. Sasaki, "Phase-locked phase-shifting laser diode interferometer with photothermal modulation," Appl. Opt. **40**, 2126–2131 (2001).
9. C. R. Mercer and G. Beheim, "Fiber-optic phase-stepping system for interferometry," Appl. Opt. **30**, 729–734 (1991).
10. T. Yoshino and H. Yamaguchi, "Closed–loop phase–shifting interferometry with a laser diode," Opt. Lett. **23**, 1576–1578 (1998).
11. T. Suzuki, T. Maki, X. Zhao, and O. Sasaki, "Disturbance-free high-speed sinusoidal phase-modulating laser-diode interferometer," Appl. Opt. **41**, 1949–1953 (2002).